Control of morphology in pattern directed dewetting of thin polymer films

Rabibrata Mukherjee,† Dipankar Bandyopadhyay and Ashutosh Sharma*

Received 24th April 2008, Accepted 4th June 2008
First published as an Advance Article on the web 21st July 2008
DOI: 10.1039/b806925e

We investigate the creation of large area mesoscale structures by controlling the dewetting pathways of thin polymer films on physically heterogeneous substrates comprising a two-dimensional (2-D) array of square pillars. Depending on the initial configuration and thickness of the film, dewetting produces a variety of both ordered and disordered structures. The substrate pattern strongly influences the dewetting pathways as well as the organization and size of the polymer structures. The key findings are: (i) the lateral confinement imposed by the substrate pattern can reduce the length-scale of the dewetted structure by one to two orders of magnitude as compared to dewetting on the same homogeneous substrate. (ii) When the polymer film is thin (<40 nm) and placed in a conformal contact with the patterned substrate, a perfect array of droplets occupying the interstitial spaces of pillar patterns is formed within a narrow range of film thickness. Nonlinear simulations show similar behavior. (iii) In contrast, for a flat polymer film resting only on the pillars and hanging freely over the channels, the dewetted droplets assemble on top of the pillars. (iv) For thicker films (>40 nm), dewetting progresses by nucleation of large holes, uncorrelated to the substrate pattern. The dewetted pattern in this case forms on multiple length-scales consisting of ~10 μm droplets resulting from the coalescence of the holes and small (<1 μm) droplets at the interstitial locations due to stick–slip of the retracting contact line.

Introduction

Morphological self-organization in dewetting of a thin polymer film is a promising method for engineering meso- and nanoscale structures over large areas. Dewetting on a defect free homogeneous substrate progresses with the formation and growth of randomly placed holes with a certain mean length-scale (λ_D).[1–21] Eventually, coalescence of holes produces an isotropic collection of droplets. The average diameters of the dewetted structures as well as their dominant wavelength depend on the initial film thickness (h_0) and interfacial tension of the polymer film.[1–18] However, randomness of the final dewetted structures and lack of long range order hinders the utility of dewetting as a viable surface patterning technique for engineering of small structures. Thus, the challenge is to bring long-range order and alignment to the dewetted structures with potential applications in fabrication of devices.[22–24] Control of dewetting structures has been investigated both theoretically[25–35] and experimentally.[36–57] For example, the structures can be aligned by rubbing the substrate or the film,[36,37] dewetting on chemically[38–45] or topographically patterned substrates,[46–50] and vertical confinement of the film under a patterned mold or stamp.[51–57]

Several theoretical studies have investigated the pathways of dewetting and pattern formation in thin films on heterogeneous substrates.[19–21,25–33] Nonlinear simulations suggested the conditions for the formation of ordered patterns such as a near commensuration between the mean length-scale of dewetting of the film (λ_D) and the imposed periodicity of the pattern (λ_P).[25–33] The existence of a parameter window for perfect templating has also been reported in related pattern forming systems such as the phase separation and ordering of block copolymers in thin films. In a recent study, Thiele *et al.*[19,20] identified the amplitude and periodicity of the chemical heterogeneity on the surface, which allow the transfer of the template pattern onto the liquid structure by dewetting. It was shown that the selected pattern is sensitive towards the initial conditions (finite perturbations), and the instability involving the transversal modes, which lead to a decay of the ridges into rows of drops, was discussed. More recently, Kao *et al.*[21] also confirmed a resonance effect in dewetting of thin films on striped patterned substrates.

Most of the studies on substrate pattern directed dewetting have been on a chemically or a simultaneously physico-chemically patterned substrate. Studies of dewetting on a purely topographically patterned, but chemically homogeneous substrate are rather sparse.[46–49] Furthermore, almost all the experiments and simulations of dewetting on topographically patterned surfaces thus far have confined attention to 1-D patterns in the form of elevated parallel stripes.[46–49] An exception is the experimental work of Xing *et al.* who considered dewetting on a 2-D array of square pillars of large dimensions (~20 μm) similar to the spinodal length-scale of dewetting.[50] Thus, the questions relating to the role of severe lateral confinement, much smaller than the spinodal length-scale in 2-D, have not been addressed. Clearly, a 2-D substrate with its interstitial spaces, columnar tops and intervening channels offers far more possibilities of self-organized ordering as compared to a 1-D substrate, which can only produce structures lacking a tight order in the direction parallel to the stripes/channels.[47,48] Thus,

Department of Chemical Engineering and DST Unit on Nanosciences, Indian Institute of Technology Kanpur, Kanpur–208016, Uttar Pradesh, India. E-mail: ashutos@iitk.ac.in; Fax: +91-512-259 0104; Tel: +91-512-259 7026

† *Present address*: Central Glass & Ceramic Research Institute, Jadavpur, Kolkata–700032, India

unlike in a 1-D geometry, substrates with a 2-D order can offer completely pre-determined sites for the formation of perfectly ordered dewetted structures.

Furthermore, the films in the earlier studies were prepared by direct spin coating on the patterned substrates, which resulted in films having variable thicknesses over the substrate protrusions and channels, depending on the coating conditions like the RPM and the solvent concentration.[46,47] While the material of the film completely fills the channels, it forms a much thinner coating on the elevated parts of the substrate. Consequently, the film first ruptures on the elevated regions of the substrate. Both the simulations[40] and the experiments[46,47] for the spin coated films show that the lateral confinement imposed by the substrate pattern is rather mild in that it is felt only when the substrate-periodicity, λ_P is of the same order or a bit less than the spinodal length-scale of dewetting, $\lambda_D \sim h^2$.[45–48] Thus, the substrate-pattern directed dewetting loses effectiveness for relatively thicker films on smaller periodicity substrates, *i.e.*, when $\lambda_D >> \lambda_P$. Both the length-scale and the order dictated by the substrate are nearly lost when the spinodal length-scale is a few times larger than the substrate periodicity. This is a serious limitation for the generation of miniaturized patterns by controlled dewetting because the spinodal length-scales are governed by long-wave instabilities. For example, the polymer films used here with thickness in the range of 20 nm to 80 nm, have spinodal length-scales in the range of 10 μm to 100 μm.[1–18]

Here, we explore conditions of film preparation other than spin coating where the lateral confinement effects of the substrate remain effective even when the pattern periodicity is much smaller than the spinodal length-scale. Thus far, the effect of the initial configuration of the film on the pattern formation has not been systematically studied. In view of the fact that self-organized dewetting is a highly nonlinear phenomenon, the initial conditions are expected to play a profound role in the determination of pathways of dewetting, selection of the site for the pattern formation, resulting pattern morphology and its order.

In this paper, we investigate dewetting of thin (10–100 nm) polystyrene (PS) films on topographically patterned substrates consisting of 2-D arrays of square posts with dimensions (~1 μm or less) that are at least one order smaller than the spinodal length-scales of dewetting. Thus, we report the effects of severe lateral confinement on the dewetting pathways and structure formation. Interestingly, a reduction in the pattern dimension by one to two orders could be obtained compared to the dewetting length-scale on a flat substrate. Further, we use uniform thickness films in this study by transferring pre-cast films onto the topographically patterned substrates. This avoids the often uncontrolled variation of the film thickness resulting from direct spin coating on patterned substrates. The role of initial configuration of the film in the pattern formation could also be studied by this sample preparation method, which allowed tailoring of two distinct initial configurations of the film. These two initial configurations correspond to: (a) a film of uniform thickness conformally adhering to the contours of the patterned substrate, and (b) periodic focal adhesion of a uniform flat film resting and adhering only to the top of the posts and hanging freely over the channels. Protocols for transferring a film onto the substrate were developed earlier to engineer the above two distinct initial configurations.[49] We thus show that the sites of pattern formation and the pattern morphology can be greatly modulated by merely controlling the initial configuration of the transferred film. Further, we investigate, by both experiments and simulations, the conditions for the formation of perfectly ordered 2-D structures and transitions to imperfect order. We thus obtain a narrow window of film thickness where near perfect order in the dewetted structure is achieved. Finally, in the case of conformal films, we also report for the first time the pathways of pattern formation for thicker films (>40 nm) on topographically patterned substrates. The rupture of the film occurs by the formation of random holes, the growth of which leaves behind droplets of polymer at the interstitial positions due to stick–slip motion of the three-phase contact line on the patterned substrate.

Results and discussion

Dewetting on a flat substrate

Stability of a thin polymer film on a defect-free, flat and smooth surface and its subsequent dewetting is determined by the nature of van der Waals interaction between the polymer and its substrate.[1–19] In this study, a thin film of PS (surface energy, $\gamma_2 \approx 31$ mJ m^{-2}) on a crosslinked PDMS (polydimethylsiloxane) surface ($\gamma_1 \approx 20$ mJ m^{-2}) is considered.[53] Wetting of a surface is characterized by its spreading coefficient defined as: $S^{LW} = \gamma_1 - (\gamma_2 + \gamma_{12})$, where γ_1 and γ_2 are the surface tensions of the substrate and the liquid, respectively and γ_{12} is the interfacial tension between the substrate and the liquid. A negative spreading coefficient, $S^{LW} \approx -12$ mJ m^{-2} for our system indicates that a thin film is inherently unstable because of the van der Waals interaction.[12] The shapes of the dewetted droplets are governed by the equilibrium contact angle (θ_E) of the polymer material on the substrate surface.

The dewetting dynamics of the floated PS films on a flat PDMS substrate were found to be similar to the well-known evolution sequence of a PS film dewetting on silicon wafer or quartz surfaces.[1–18] Fig. 1 shows the dewetting sequence for a 24 nm thick PS film on a flat crosslinked PDMS substrate. For the 24 nm thick film, the onset of instability was manifested after solvent vapor exposure for 85 seconds with the appearance of a random collection of fairly uniform sized, isolated holes (Fig. 1A), which grew in size and numbers as dewetting continued (Fig. 1B, 3 minutes exposure). Growth of the holes with prolonged solvent vapor exposure led to the coalescence of the rims adjacent to the holes and the formation of polymer ribbons after ~7 minutes (Fig. 1C) of solvent vapor exposure. The polymer ribbons finally broke up into isolated polymer droplets (Fig. 1D, 16 minutes of exposure) in the final stages of dewetting. After this stage, there was no further change in the morphology of the structures over a time period of a few hours. AFM scans of the fully dewetted structures for a 24 nm thick PS film (Fig. 1E) with cross sectional analysis showed the contact angle between the droplet and the PDMS substrate to be 38.9 (±2.3)°. The contact angle was found to lie in a narrow range, 36.2–40.8°, for all the droplet sizes obtained in this study for different film thickness.

Change in the initial film thickness (h_0) on a flat surface produced no change in the dewetting pathway, but altered the length and the time scales. For example, the first holes appeared after 20 s, 45 s, 85 s, 120 s, 3.5 min, 5 min and 18 min for films

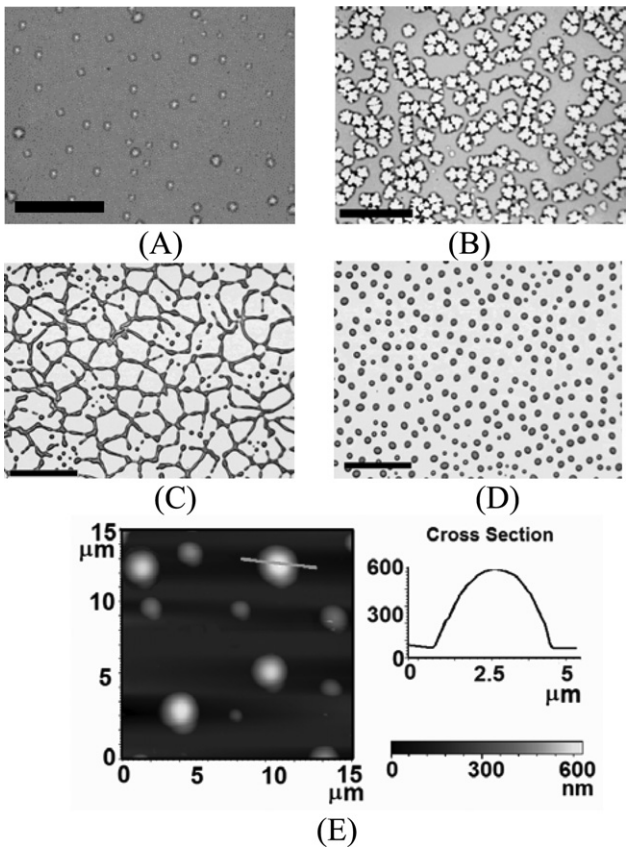

Fig. 1 Morphological evolution of a 24 nm thick PS film on a flat, smooth crosslinked PDMS surface during different stages of solvent (toluene) vapor assisted dewetting, after vapor exposure for (A) 85 seconds (initiation of random holes), (B) 3 minutes, (growth of the holes), (C) 7 minutes (coalescence of growing holes leading to the formation of polymer ribbons) (scale bar 30 microns) and (D) 16 minutes (formation of isolated dewetted droplets). (E) AFM scan of the dewetted structure, showing the cross section of an individual droplet. The scale bar is 50 μm in all the images except (C).

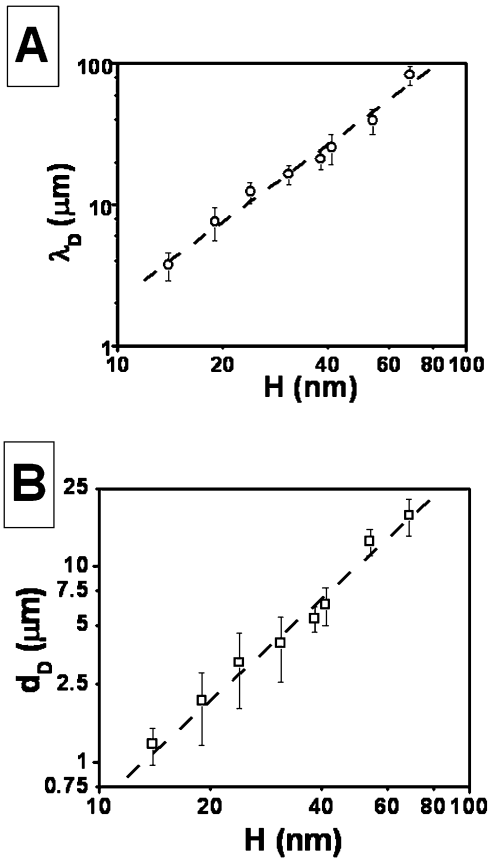

Fig. 2 (A) Plot of the length-scale of the dewetted structures (λ_D) as a function of initial PS film thickness (h_0). The slope of the linear best fit line is 1.819 ± 0.156. (B) Plot of the average droplet diameter (d_D) as a function of initial film thickness (h_0).

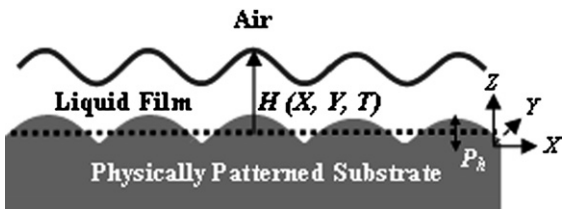

Fig. 3 Schematic diagram of a thin film placed conformally on a topographically patterned substrate. The local film thickness and the height of the pillar are denoted by $H(X,Y,T)$and P_h, respectively.

having initial thicknesses of 11, 17, 24, 31, 41, 54 and 69 nm, respectively. Complete dewetting was observed after 4, 8.5, 16, 23, 39, 85 and 140 min of solvent vapor exposure for the films with initial thickness 11, 17, 24, 31, 41, 54 and 69 nm, respectively.

The variation of the length-scale and the average droplet diameter of the final dewetted structures as a function of the initial film thickness (h_0) are shown in the plots in Fig. 2A and B, respectively. The best fit to the data in Fig. 2A shows a functionality of λ_D and h_0 as $\lambda_D \sim h_0^{1.819\pm0.156}$, which is close to the theoretically predicted and experimentally observed scalings.[1–16] The value of an effective Hamaker constant corresponding to these data is obtained as $A_E = -5.183\ (\pm\ 2.046) \times 10^{-20}$ J, based on the wavelengths of the dewetted droplets in Fig. 2A.

Dewetting on patterned substrates

The geometry of the system under investigation, where a thin polymer film is dewetting on a topographically patterned substrate, is schematically shown in Fig. 3. In the context of dewetting on a 2-D patterned substrate comprising an array of square pillars (type 1 and type 2 substrates, defined in the Experimental section), we define a perfectly ordered structure to be the one where all the pillar-tops and/or the channel intersections are occupied by isolated PS droplets. If some of the sites remain vacant or some of the adjacent droplets are interconnected, the structure has some disorder. Further, even in the case of a perfectly ordered structure, perfect filling occurs when the dimension of each dewetted droplet corresponds to the largest dimension that can be accommodated at a specific site. Thus, for type 1 or type 2 substrates, the dimensions of the roof of the posts or the size of the channel intersections govern perfect filling. This will correspond to a droplet having a base diameter of ~750 nm for a type 1 substrate, where both the roof dimensions as well as the channel intersections are about 750 nm

square. In addition, the final droplet geometry is also governed by the equilibrium contact angle of the dewetting polymer on the substrate material. If the droplet sizes are smaller than the largest possible dimension, under-filling of the sites occurs.

Dewetting of conformally adhering films

Regimes of film rupture: effect of film thickness

Film rupture correlated with substrate pattern: thin to moderate thickness films. Fig. 4 shows the influence of initial PS film thickness on the final morphology of the dewetted patterns on a type 1 substrate (inset A1) where the polymer film is conformally adhering to the underlying substrate (Fig. 4A). The nature and extent of conformal adhesion was verified by superimposing the AFM line scans of the floated film (dotted line in inset A2) on the line scan of the bare substrate (continuous line in inset A2).

Fig. 4B–E shows the influence of initial film thickness on the dewetted morphology. Fig. 4B displays the final dewetted morphology of an 11 nm thick PS film, where the droplets occupy only some random interstitial positions adjoining the pillars and other sites remain vacant. The base diameter (d_b) and height of the dewetted droplets (h_d) are $\sim$422 $\pm$ 19 nm and 63.3 $\pm$ 4.2 nm respectively, with $\theta_E \approx 36.9 \pm 2.1^\circ$ between the droplet and the substrate. Thus it is a disordered, as well as an underfilled structure. Fig. 4C shows that the dewetted droplets from a slightly thicker, 17 nm thick film occupy every available interstitial space. The dimensions of the droplets are: $d_b \approx 441.5 \pm 5.1$ nm, $h_d \approx 68.3 \pm 1.3$ nm and $\theta_E \approx 37.4 \pm 1.3^\circ$. This is a perfectly ordered, but underfilled structure, as the base diameter is less than the largest diameter, $\sim$750 nm, that can be accommodated at each interstitial space. Fig. 4D shows perfect ordering as well as near optimal filling for an initial film thickness of 24 nm. The base diameter of the droplets is $\sim$729 $\pm$ 3.1 nm, which corresponds to the largest droplet that can be accommodated at each location ($\sim$750 nm). Other droplet dimensions are: $h_d \approx 113.3 \pm 1.3$ nm, $\theta_E \approx 40.4 \pm 0.3^\circ$. Fig. 4E shows that increasing the film thickness further to 31 nm leads to loss of order because of overflow, as the droplets are seen to spill out along the channels and some of them remain connected with neighboring droplets. Thus, the experiments suggest that dewetting of films on a 2-D patterned substrate can lead to perfect ordering and perfect filling only for a narrow range of initial film thicknesses. On a type 1 substrate, perfect ordering of the dewetted structures is observed for films with initial thicknesses in the range of $\sim$15 nm to 25 nm, with perfect filling for $\sim$24 nm thick films.

To uncover the details of the dewetting pathways leading to imperfect or perfect ordering we performed a series of 2-D and 3-D nonlinear simulations based on the formalism employed previously.[13,25–33] The details of the hydrodynamic model are provided separately at the end of this manuscript in the Methods section. Here we consider the spatiotemporal evolution of a thin liquid film of constant thickness, which is conformally placed on a topographically patterned substrate as schematically shown in figure 3. The thin film equation (eqn (1)) governing the stability, dynamics and surface morphology of a thin Newtonian film was derived based on the continuity and Navier–Stokes equations and rendered dimensionless for a more compact representation after introducing a set of scaling parameters.[13,25–33] The

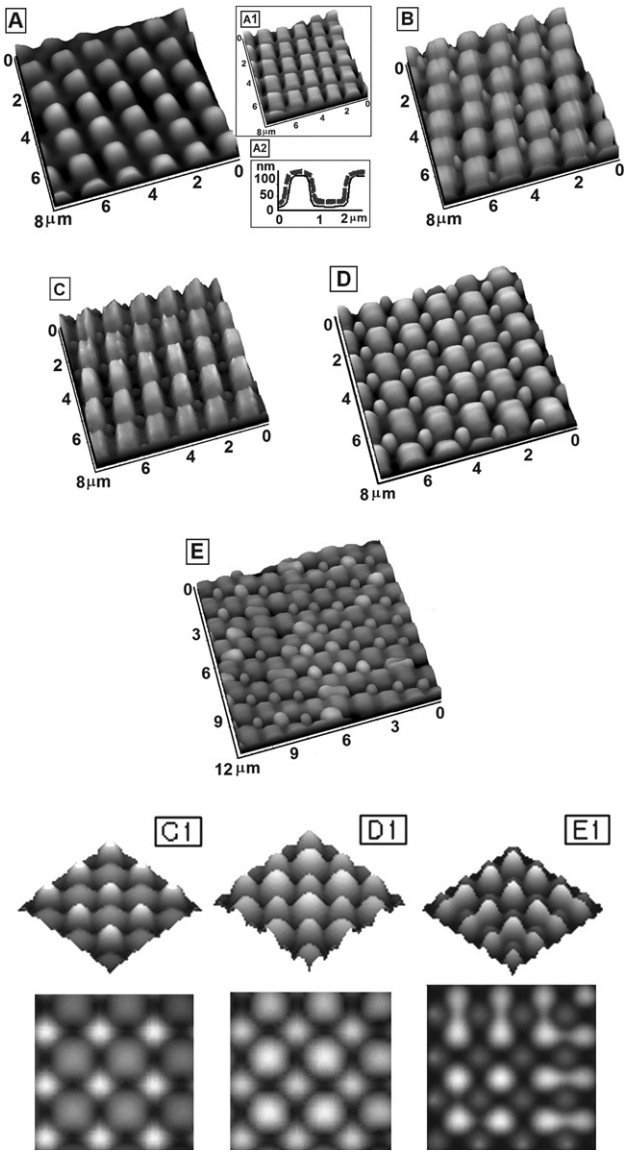

Fig. 4 (A) A floated PS film conformally adhering to a patterned type 1 substrate, comprising an array of square pillars. Inset A1 shows the substrate morphology and inset A2 shows the line profile of the substrate and the film. (B–E) Morphology of the final dewetted structures with the change in the initial film thickness on a type 1 substrate. (B) Imperfect ordering with some missing droplets for an 11 nm film, (C) perfectly ordered but underfilled structure formation for a 17 nm thick film, (D) perfectly ordered and filled array for a 24 nm thick film and (E) distorted, overfilled structure with occasional oversized or interconnected droplets for a 31 nm thick PS film. (C1–E1) are simulation pictures of the dewetted morphology for $T_R = h_0/P_h = 0.27$, 0.3125 and 0.5, respectively.

nondimensional equation thus obtained was numerically solved to obtain the 2-D and 3-D morphologies. The first term of the thin film equation (eqn (1)) represents the time derivative of the nondimensional local height $H(X,Y,T)$, the second term represents the Laplace pressure because of the curvature at the interface and the third term represents the interaction because of the intermolecular forces. The topography of the substrate was modeled as a smoothly varying periodic function, rather than the sharp pillar geometry because of likely numerical artifacts

inherent in computing flows around steep corners. However, many of the key features of the experiments including transition from underfilling to overflow could be qualitatively reproduced in the simulations. In simulations, the dimensionless ratio ($T_R = h_0/P_h$) of the film thickness (h_0) to pillar height (P_h) is the parameter that reflects the influence of the initial film thickness. Increase in the value of T_R corresponds to a larger liquid mass per unit area. Fig. 4C1–E1 show the equilibrium morphologies obtained from simulations varying T_R at a constant pattern periodicity (λ_P), where λ_P is same as for the type 1 substrates employed in the experiments. λ_P is less than the spinodal length-scale (λ_D). Simulations indeed show (Fig. 4C1–E1) the experimental transitions from underfill to perfect fill to overflow of structures (4C–E). Ordered droplets are formed at the interstitial spaces of the patterned substrate for very small values of T_R (= 0.27) as seen in Fig. 4C1. The vertical heights of the isolated droplets in this case are smaller than the posts and the dewetted droplets underfill the interstitial space, as observed in the experiments (Fig. 4C). When T_R is increased to 0.3125, the dewetted morphology now shows nearly a perfect ordering and filling of the droplets, resembling the patterns obtained experimentally (Fig. 4D). Fig. 4E1 shows that when T_R (= 0.5) is further increased, the droplets have higher heights than the posts and the base fills up the entire interstitial space and a part overflows onto the adjacent channels forming some connected droplets. This scenario corresponds to the experimental observations for a thicker film in Fig. 4E.

The experimental and simulated results in Fig. 4 clearly suggest that the amount of polymer loading per unit cell influences the dewetting pathway and the resulting morphology. The simulations also reveal that there are two different pathways of dewetting as the ratio of the film thickness to pillar height is varied. Fig. 5 shows the simulated 2-D and 3-D evolution images when T_R= 0.5. At short times, lower Laplace pressure at the valleys leads the liquid to flow down the hills to fill up the channels (Fig. 5b). In this case, high T_R ensures availability of sufficient liquid mass to fill up the valleys completely and the patterned substrate becomes submerged in a pool of liquid at the intermediate stages of dewetting (Fig. 5b). Thereafter, the smaller local film thickness increases the strength of the van der Waals interaction locally on top of the pillars where the film ruptures [solid line 2 in plot 5A and Fig. 5c]. Following this, as the three-phase contact line tries to achieve equilibrium, the holes progressively grow with time [line 3 in plot 5A and Fig. 5d] and their rims coalesce to form droplets in the channels (Fig. 5e and 5f). Long time morphology shows that some of the droplets become isolated after getting disconnected from the neighbors and others remains connected through liquid bridges spanning over the channels (Fig. 5f).

In contrast to the above situation, simulations uncovered another pathway of dewetting leading to the near perfect ordering and filling at moderate film thickness to pillar height ratio. For example, simulations in Fig. 6 show the dewetting pathway of a polymer film conformally placed on a solid substrate for T_R = 0.3125 (solid line 1 in plot 6A and Fig. 6a). This initial configuration ensures higher Laplace pressure at the top of the pillars and therefore, the fluid flows downhill to fill the channels in the initial stages of dewetting. The film first ruptures and dewets from the sides of the pillars (solid line 2 in Fig. 6A

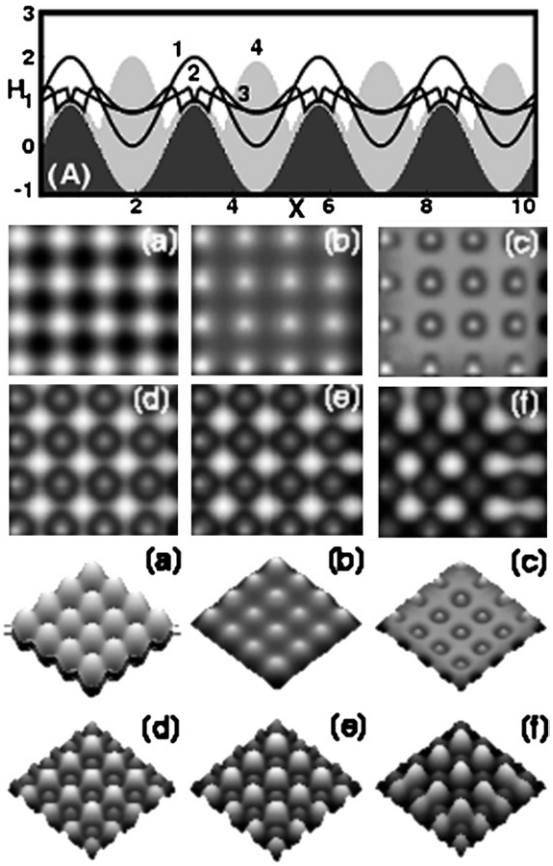

Fig. 5 2-D and 3-D nonlinear simulations when $T_R = 0.5$. The solid lines (1)–(3) in the plot (A) show the initial configuration of the film and the intermediate stages of the evolution, and the filled gray profile (4) shows the final configuration. Images (a)–(f) in the first two rows show the top view of the interfacial morphologies and the images (a)–(f) in the last two rows show the 3-D surface profile. The value of the effective Hamaker constant used for these simulations is $A_E = 5.45 \times 10^{-20}$J. In the grayscale images, darker shades of gray represent the lower film thickness regions.

and Fig. 6b). The uncompensated Young's force leads to the movement of the contact line and the liquid accumulates in the form of droplets within the channels. Although in the intermediate stages of evolution, the droplets at the interstitial spaces between the pillars remain connected (Fig. 6c and d), near equilibrium, they are pinched off from each other and form islands of droplets at the channel intersections (filled light grey region in plot 6A and Fig. 6e). The high-energy tiny droplets at the top of the posts coalesce with the drops in the valleys during the late stage of ripening. The final morphology shows near perfect ordering and filling (Fig. 6f).

Experiments also confirm that the film ruptures on every pillar (Fig. 7A) and subsequently, all the polymer migrates into the channels (Fig. 7B), exposing the tops of the pillars (inset of Fig. 7B). The final stages of structural reorganization produce a perfectly filled and ordered structure by the migration of polymer from the channels to the corners (Fig. 7C), which apparently corresponds to the thermodynamically preferred configuration.

Film rupture uncorrelated to substrate pattern: thick films. In contrast to the dewetting sequence observed for ultra- and

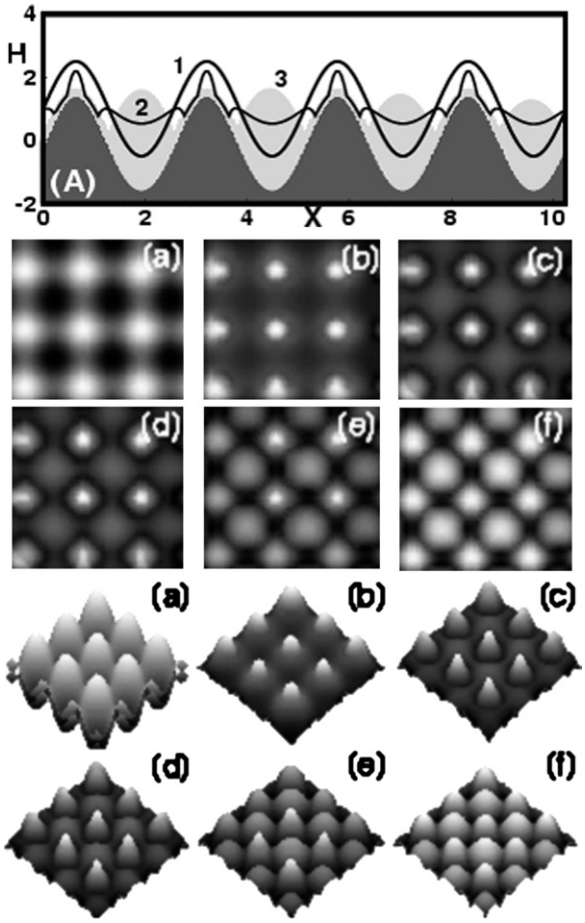

Fig. 6 2-D and 3-D nonlinear simulations when $T_R = 0.3125$. The solid line (1) in the plot (A) shows the initial configuration of the film, the solid line (2) the intermediate stages of the evolution, and the filled gray profile (3) shows the equilibrium configuration. Images (a)–(f) in the first two rows show the top view of the interfacial morphologies and the images (a)–(f) in the last two rows show the 3-D surface profiles. The value of the effective Hamaker constant used for these simulations is $A_E = 5.45 \times 10^{-20}$ J. In the grayscale images, darker shades of gray represent the lower film thickness regions.

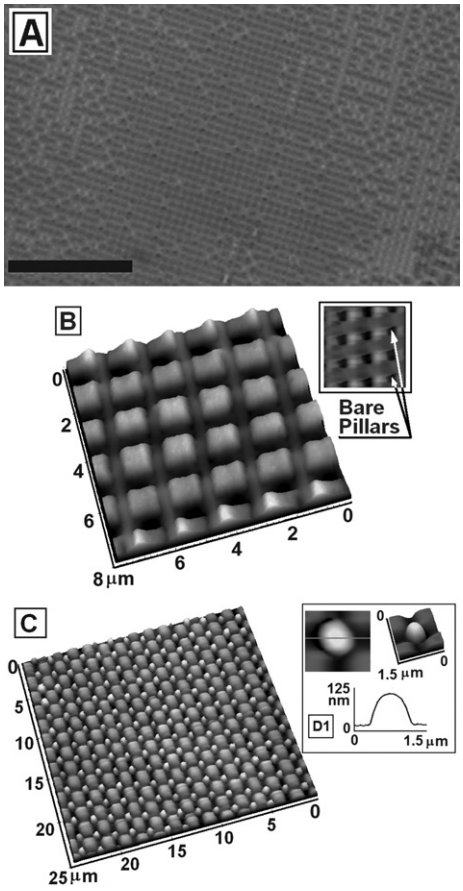

Fig. 7 Dewetting sequence of a 24 nm thin PS film on a type 1 substrate. (A) Large area optical micrograph shows that the film has ruptured along the periphery of each pillar roof, after 1 minute of exposure to solvent vapor. Scale bar is 40 μm. (B) After 3 minutes, the pillar roofs are denuded, as the polymer fills the channels. AFM phase contrast image in the inset shows the substrate is exposed on the pillar roofs (dark color). (C) After 5 minutes of exposure, a perfectly ordered and filled structure is obtained. Inset shows AFM line scan of a drop profile.

moderately thin films on a type 1 substrate, a completely different dewetting pathway is seen for the films with thickness >40 nm. Fig. 8 shows the evolution of a 69 nm thick film dewetting on a type 1 substrate. As seen in Fig. 8A, dewetting was initiated with the formation of random holes, in a fashion similar to dewetting of a film on a flat substrate. This is unlike the case witnessed in thin to moderate thickness films where the film rupture is correlated to the underlying pattern (Fig. 4–7).[46–50] Interestingly it is seen in Fig. 8B that the periphery and the rims of the holes become aligned with the substrate patterns and consequently, the holes appear rectangular rather than circular. The underlying substrate pattern is also clearly visible in the same figure, particularly inside the holes from where the film has already dewetted. The AFM scan of the dewetted portion inside a hole reveals the fine structure of the polymer left behind by the moving contact line (Fig. 8C). The three-phase contact line (film–substrate–air) of a growing hole leaves behind a droplet of polymer at each interstitial corner on the patterned substrate. This observation sheds new insight on the dewetting dynamics of thicker polymer films on physically heterogeneous substrates. The striking features of this phenomenon are: (i) the dewetting of the film is initiated by the nucleation of random holes non-correlated to the substrate patterns, (ii) the motion of the three phase contact line of a growing hole is of stick–slip type, and (iii) as the contact line moves to the next pillar it leaves behind an isolated polymer droplet at each interstitial corner location, because it is most difficult to pull any residual liquid from there. With progress of dewetting, the rims of adjoining holes touch each other and form ribbons (Fig. 8D) similar to those seen for dewetting on a flat surface (Fig. 1C).[1–19] Subsequently, the polymer ribbons decay into randomly located large droplets, as can be seen under the view of a low magnification optical microscope (Fig. 8E). The first inset E1 to the figure (a higher resolution optical micrograph) shows the topographically patterned substrate around a dewetted polymer droplet. An AFM scan of the exposed areas of the sample reveals the formation of a perfectly ordered and perfectly filled structure (inset E2). The average base diameter of the droplets is $\sim 738 \pm 2.1$ nm, which is very close to the maximum dimension of a PS

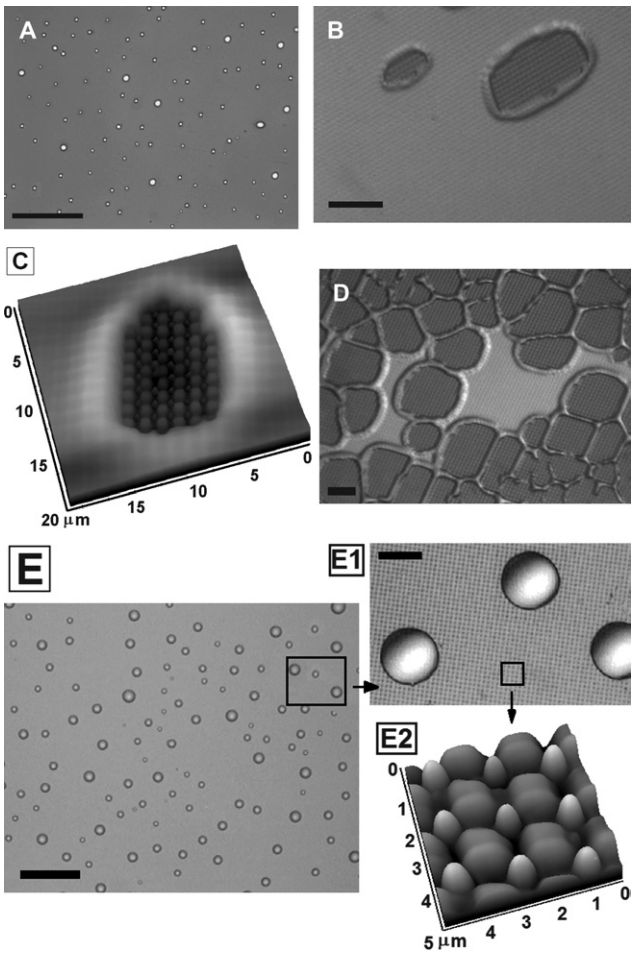

Fig. 8 Dewetting pathway of thicker films (~69 nm) on a patterned surface, with nucleation and growth of random, large holes. (A) A large area optical micrograph showing the formation of random holes (scale bar 150 μm), (B) high magnification optical micrograph showing the exposed substrate patterns within a hole (scale bar 15 μm), and (C) an AFM image of a hole, revealing the presence of small polymer droplets at each interstitial position on the substrate within a hole. For images (A)–(C), exposure time is 4 minutes. (D) Formation of polymer ribbons after solvent vapor exposure for 11 minutes (scale bar 15 μm). (E) Large area optical micrograph showing large polymer droplets, after solvent vapor exposure for 35 minutes (scale bar 100 μm). The inset E1 is a higher magnification optical micrograph, showing that the large polymer droplets are resting on a cross patterned substrate (scale bar 15 μm) and the AFM scan in inset E2 shows the presence of polymer droplets at the interstitial positions on the substrate patterns, forming a perfectly ordered and filled pattern.

droplet that can be accommodated at an interstitial location of a type 1 substrate. The observations in Fig. 8 show the co-existence of patterns at two different length-scales: (a) the large, randomly distributed droplets that are typically about 10 μm or more in diameter produced by the coalescence of the holes, and (b) an ordered array of sub-micron droplets, formed due to the stick–slip motion of the retracting contact line, where the size of the droplet nearly equals the base area available at channel intersections. Similar evolution sequences were also observed for 41 nm, 54 nm and 78 nm thick films (images not shown).

In addition to the pathways of dewetting and the resulting morphologies, the timescale of dewetting on a patterned substrate was also found to be strongly influenced by the substrate patterns. For films thinner than 31 nm, where dewetting is correlated to the underlying pattern, the overall dewetting dynamics became faster when compared to those on a flat surface. For example, a 31 nm film fully dewets in about 5.5 minutes on a type 1 substrate, in contrast to 23 minutes taken on a flat substrate for a film of the same thickness. Faster dewetting is also observed for 11 nm (1 *vs*. 4 min), 17 nm (1.8 *vs*. 8.5 min) and 24 nm thick films (3.5 *vs*. 16 min). However, for films thicker than 40 nm, where the contact line undergoes stick–slip on the patterned substrate, the speed of dewetting became significantly slower compared to dewetting on a flat substrate. The time taken for complete dewetting for a 41 nm thick film rose to 62 minutes on a type 1 substrate, compared to 39 minutes on a flat surface. Similar enhancement in the timescale was observed for a 54 nm film where the time of dewetting increased from 85 minutes on a flat surface to ~150 minutes on a type 1 substrate. Similarly, a 69 nm thick film dewetted in 225 minutes on a patterned surface as compared to the 140 minutes it took on a flat substrate. The slower dynamics of dewetting on a patterned substrate in this case can be attributed to the additional resistance encountered by the dewetting front which is periodically pinned by the channels and detaches only by shedding some of its mass in the interstitial spaces.

Influence of pattern dimension on final structures. The perfectly ordered and filled structures in Fig. 5D are obtained from the dewetting of a 24 nm thick PS film on a type 1 substrate. Creation of such highly ordered, defect-free structures over areas spanning several square centimetres shows the promise of controlled dewetting as a patterning technique. For a 24 nm thick film, the typical droplet diameter is ~3.4 ± 0.84 μm (Fig. 2B) and the structure periodicity is ~11.4 ± 1.22 μm on a defect-free flat surface (Fig. 2A). In contrast, an average droplet diameter of ~729 nm and periodicity of ~1.5 μm is achieved here by pattern directed dewetting of a film of the same thickness on a type 1 substrate. The topographic patterns impose severe lateral confinement to the dewetting process, resulting in a feature size commensurate with the substrate dimensions rather than the length-scale of the instability on a flat surface. Dewetting on a topographically patterned substrate can thus reduce the lateral dimensions of the dewetted structures by at least one order of magnitude, in addition to inducing the pattern alignment and ordering.

The influence of the substrate pattern dimension or the extent of lateral confinement on the final dewetted structure is further demonstrated when a type 2 substrate (inset to Fig. 9) is used. When a 24 nm thick PS film is dewetted on this substrate, a perfectly ordered and filled structure identical to the one shown in Fig. 4D is readily achieved (Fig. 9). In this case, the average diameter of the droplets was found to be ~348.3 ± 12 nm, which is again commensurate with the corner size of 400 nm square. The results are important from the point of view of miniaturization of patterns, as by using a substrate with smaller patterns, further reduction in periodicity and size of the dewetted structures could be achieved. Variation in the film thickness again resulted in the shifts of the pattern morphology similar to that

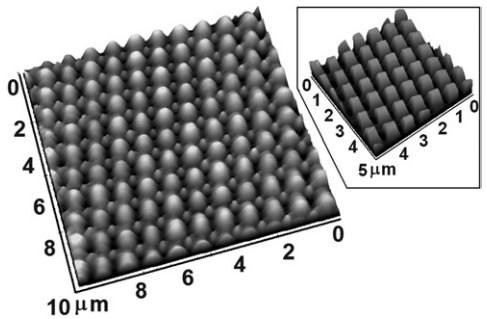

Fig. 9 Perfectly ordered and filled structure obtained by dewetting of a 24 nm thick film on a type 2 substrate The average droplet size is ~348 nm.

observed in Fig. 4. Similar qualitative dependence of final ordering and filling on film thickness on type 1 and type 2 substrates can be attributed to the morphological similarity of the two types of substrate. This, in simple terms, can be explained as a nearly identical relative ratio between the area of the substrate covered by the pillars and that in the channels for both type 1 and type 2 substrates.

Interestingly, dewetting of a spin coated film shows far less effect of the lateral confinement induced by the substrate topography.[31,38–48,50] Spin coating produces a periodic variation of the film thickness while completely filling the channels on the substrate.[46,47] The film breakup is now governed by the spinodal length-scale, rather than the substrate periodicity, and the order imposed by the substrate is lost.[40,47] However, as is shown here, the length-scale of the dewetted structures in a transferred film can be identical to the substrate periodicity even when the spinodal length-scale on a flat substrate is much larger than the substrate periodicity. Clearly, the wavelength of the fastest growing mode[1–21] is greatly influenced by the substrate patterning, especially when the pattern periodicity is less than the spinodal length-scale.

Dewetting on more complex patterns. So far, we have presented results on the patterned substrates having a 2-D array of square pillars. In this section, we show how more complex, ordered dewetted structures can be created using a substrate with intricate patterns. Here, a type 3 substrate (shown in inset A2 of Fig. 10), comprising arrays of rhombic zones (marked as "E" in the inset) having 800 nm long sides (~40 nm high) and separated by channels 400 nm wide on all sides, marked by "F" and "G" in the inset, is used as the substrate for dewetting. Fig. 10A shows the initial morphology of a 31 nm thick floated PS film, conformally adhering to the substrate. The initial rupture takes place along the intersections of raised spikes that separate different domains, because the Laplace pressure as well as the total stress in the film are maximum at these points. The local rupture spots propagate further along the boundaries of all the different zones and the film gets split into several parts. A strip of the polymer accumulates along each long channel, while each rhombic and trapezoidal zone (marked by "E" and "F" respectively) contains a detached, isolated part of the film confined entirely within the domains. All the dimensions of the confining zones, except that along the length of channels "D" are smaller than 16.4 μm, the spinodal length-scale of instability for a 31 nm thick film

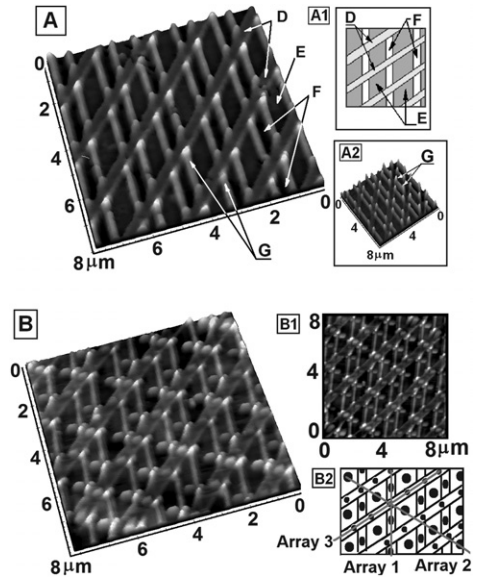

Fig. 10 (A) A 31 nm thick PS film adhering conformally to the complex patterned substrate shown in inset A2. Inset A1 explains the morphology of the substrate patterns. (B) After solvent vapor exposure for 7 minutes, the film dewets, forming a "star" shaped array of PS droplets (explained in the line diagram in inset B2). The inset B1 shows a 2-D AFM scan of the same structure.

(Fig. 2A). Thus, within respective confining areas, each film segment undergoes dewetting separately forming a droplet at the centre of each rhombic or trapezoidal zone, except in the long channels, where the long strips of the film break down along the channel, forming an array of aligned droplets along the channels. A schematic drawing in one of the insets to Fig. 10B depicts the arrangement of the final pattern which comprises a complex, yet very regular "star" shaped array of the dewetted droplets.

Dewetting of a focally adhering film

In this section, the influence of the initial film morphology on the patterned substrate is demonstrated. In all the discussion so far, PS films in conformal contact with the underlying substrate pattern have been used. Here we discuss the dewetting of a 24 nm thick floated PS film which is in focal adherence with a type 1 substrate. In this configuration, the overall morphology of the film is nearly flat as the film comes in contact only with the raised protrusions (post roofs) of the patterned substrate and hangs freely over the other areas, as can be seen from the superimposed AFM line scans in the inset of Fig. 11. A thickness of 24 nm is chosen for comparison because perfect ordering and filling has been achieved with films of this thickness for conformally adhering films. When such a free hanging film is exposed to the solvent vapor, the rupture is initiated at the areas that hang freely over the channels. This is in contrast to the initial rupture on the pillars for a conformally adhering film (Fig. 6 and 7A). The higher effective Hamaker constant and zero viscous hindrance at the freely hanging areas of the film, compared to other areas of the PS film, engender the first rupture of films there. It is also known theoretically that thin free films rupture rather explosively compared to films supported on a solid substrate.[58] Consequently

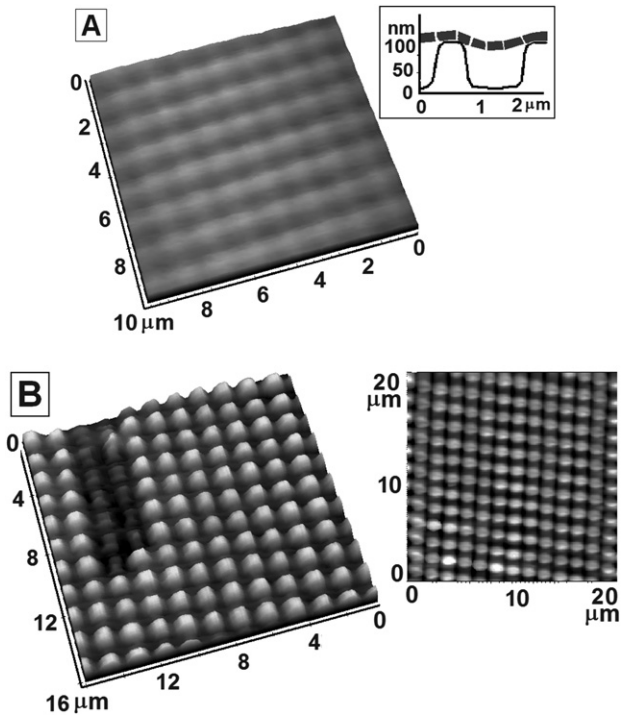

Fig. 11 (A) A 24 nm thick PS film before dewetting, in "focal adhesion" on a type 1 substrate. Inset shows the film (dashed line) in contact with the raised protrusions of the substrate (continuous line) and freely hanging over other intervening areas. (B) The dewetted droplets are positioned on top of each pillar roof. A portion with a slight defect is deliberately shown to distinguish between the dewetted droplets and the underlying pattern below, which can be seen at the place where the dewetted droplets are not placed on the pillar tops. Inset shows an area with a perfect array.

the ruptured film snaps to the top of the neighboring pillars and with continued solvent exposure, the polymer further moves towards the centre of the pillars, ultimately forming a droplet on top of each pillar, as shown in Fig. 11B.

The image (Fig. 11B) has a slight defect as due to tearing of the initial film over a small zone, the dewetted droplets have not formed over some of these columns (appearing as darker zones on the far side of the image), exposing the underlying substrate. This image is deliberately attached, in order to convince the readers that the droplets indeed form on top of the pillar roofs, which is otherwise difficult to clearly distinguish in case of a defect-free image like the one shown in the inset of Fig. 11B. Thus, for a hanging film configuration with a 24 nm thick PS film on a type 1 substrate, a perfectly ordered structure is yet again achieved, where each pillar roof is occupied by a PS droplet having base diameter $\sim$687 $\pm$ 6 nm. This droplet diameter corresponds to nearly the largest droplet diameter (of $\sim$750 nm) that can be accommodated on the roofs of the pillars.

Methods: experimental and theory

Fabrication of the patterned substrates

The patterned substrates were made by Adhesion Assisted Imprinting of crosslinked PDMS (sylgard 184, Dow Chemicals, USA), following methods described elsewhere.[59–61] The topography of the patterned substrates are shown in the inset of Fig. 4A ("type 1" substrate), inset of Fig. 7 ("type 2" substrate) and inset A2 of Fig. 10 ("type 3" substrate). The type 1 and type 2 substrates consist of arrays of square posts. The periodicity of the posts along both the axial directions is 1.5 μm in the case of a type 1 substrate and 800 nm in the case of a type 2 substrate. The roof dimensions of the posts are 750 nm × 750 nm and 400 nm × 400 nm, respectively for these two types of substrates. These posts are surrounded by 750 nm and 400 nm wide channels on all four sides, respectively. Another type of topographically complex substrate used (type 3) comprised arrays of rhombic zones (marked as "E" in the inset of figure A2 of Fig. 11), having 800 nm long and $\sim$40 nm high side walls. The rhombuses are separated by $\sim$400 nm wide channels on all sides, marked by "D" and "G" in the inset. While channels marked "D" are continuous and long, those marked "G" are small trapezoidal zones, having dimensions $\sim$300 nm (wide) × 800 nm (long), separating adjoining rhombic zones. The method of creation of this particular type of substrate can be found in detail elsewhere.[61]

Polystyrene thin film of uniform thickness on the patterned substrates

Mono-dispersed polystyrene (PS) (Sigma Aldrich, UK) was used for the experiments (M_n = 280 K g mol^{-1}, polydispersity index (PDI) <1.1, $T_G \approx 103$ °C). Direct spin coating of PS solution on a topographically patterned surface leads to non-uniformity in film thickness or rupture of the film during spinning itself (for very thin films) due to the presence of physical heterogeneity on the substrate.[46,47] In order to maintain uniform thickness of the films on the patterned substrates, the PS films were transferred onto the substrates. Towards this end, films were first spin coated from their solution in HPLC grade toluene (E. Merck) onto thoroughly cleaned smooth silicon wafers. The thicknesses of the PS films were measured using a nulling Ellipsometer (EP3, Nanofilm). The experiments reported in this paper were done with PS films of thicknesses (h_0) of 11 ($\pm$ 0.6), 17 ($\pm$ 0.8), 24 ($\pm$ 0.5), 31 ($\pm$ 0.6), 41 ($\pm$ 1.2), 54 ($\pm$ 1.1), 69 ($\pm$ 1.3) and 78 ($\pm$ 0.5) nm.

The PS films, after air drying for 60 minutes, were detached from the silicon wafers by carefully floating on water (Fig. 12). The freely floating PS films on water surface were picked up by the patterned substrates. The orientation and lifting speed of the substrate while capturing the freely floating film from the water surface significantly influenced the morphology of the PS film on the patterned substrate as schematically shown in Fig. 12. A slow vertical removal of the substrate resulted in a PS film which adhered rather closely to the contours of the substrate. This initial configuration will be referred to as the "conformal adhesion" (inset A2 of Fig. 4A). In contrast, when the substrate was kept horizontal and the floating film was rapidly pulled out, it resulted in the "focal adhesion" or a "free-hang" configuration, (inset of Fig. 11). This method produced a flat film which adhered only to the top of the posts and remained freely suspended in air over the channels. Most of the results on dewetting on patterned substrates reported in this paper (Fig. 4 to 10) are based on conformally adhering films, while in Fig. 11, the "free hanging" initial

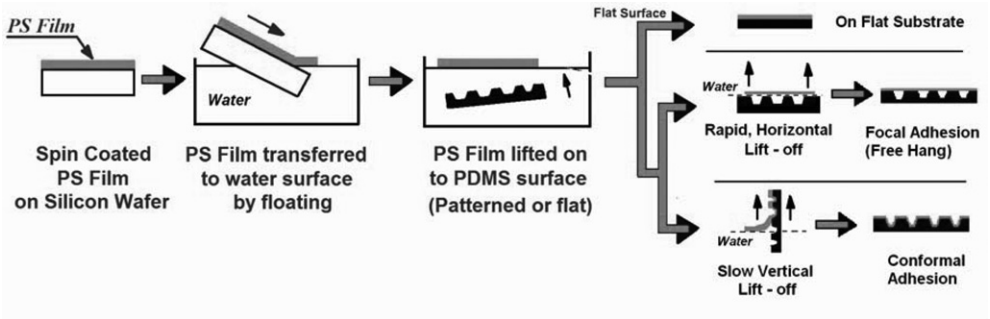

Fig. 12 Schematic of the protocol used for floating the thin polystyrene (PS) film on water and its' subsequent transfer onto patterned or flat cross-linked polydimethylsiloxane (PDMS) substrates.

condition of the film has been used to demonstrate the influence of initial configuration on the final morphology of the patterns.

In order to remove any residual amount of water that might remain entrapped during the transferring operation, the films were air dried for 18 hours after transferring and subsequently, annealed at 60 °C for 24 hours in a low vacuum oven to release any residual stresses. Each sample thus prepared was scanned using an AFM (Pico Plus, Molecular Imaging) to ascertain the exact film morphology on the patterned substrate.

To understand the influence of the substrate pattern on dewetting morphology and length-scales, results for the patterned substrates are contrasted with dewetting on flat substrates of the same material (cross-linked PDMS). To maintain uniformity of the sample preparation conditions, experiments on the flat substrates also employed transferred films using the same protocol described above. Films were never directly spin coated on to any of the substrates.

Dewetting methodology and *in situ* tracking

The dewetting of the films was engendered by solvent vapor exposure. For this purpose, the samples were placed in an air tight chamber pre-saturated with toluene vapor, which is a good solvent for PS. Exposing a polymer film to its solvent vapor effectively reduces the effective glass transition temperature due to the penetration of the solvent molecules into the polymer matrix. The experimental chamber had a glass cover for viewing and was mounted on the X-Y-Z stage of an optical microscope (Leica DMLM) for *in situ* observations, using white light and reflection mode. The samples were withdrawn from the chamber after complete or partial dewetting for further detailed analysis using an AFM, where imaging was performed in the tapping mode with silicon cantilevers (Mikromasch, Estonia).

AFM was also employed to measure the equilibrium contact angle of the dewetted droplets. The "shadowing effect" was minimized by superimposing cross sectional analysis obtained by altering the directions of scans.

Non-linear simulations: hydrodynamic model

We consider the polymeric liquid film to be isothermal, incompressible and Newtonian. The substrate was modeled as having a periodic sinusoidal topography. The system is shown schematically in Fig. 3. In simulations, the sharp corners and steep slopes of the experimental posts were suppressed because of the numerical artifacts that are generated and also because of the use of the widely employed "lubrication" or "small-slope" approximation. The surface topography was modeled as a function of the position coordinates, $Z = BF(X,Y)$, where B is the nondimensional amplitude ($P_h/2h_0$) of the roughness function $F(X,Y)$. In the simulations, $F(X,Y)$ is considered as a sinusoidal wavelike function [sin(KX) + sin(KY)] of periodicity interval $Lp = 2\pi/K$. The following non-dimensional thin film equation, derived from the long-wave Navier–Stokes equation with the boundary conditions, (a) no slip and impermeability at the film–substrate interface, and (b) zero shear and normal stress balance at the film–air interface, governs the dynamics of a thin liquid film on a rough surface subjected to the excess intermolecular interactions:[31]

$$\partial H/\partial T + \nabla[(H - BF)^3\nabla(\nabla^2 H)] - \nabla[(H - BF)^3\nabla\Phi] = 0 \quad (1)$$

In eqn (1), $H(X,Y,T)$ is the non-dimensional local height of the film scaled with mean film thickness, h_0, and measured from the datum $Z = 0$. The nondimensional conjoining pressure Φ is a function of the local film thickness, $\chi = [H(X,Y) - BF(X,Y)]$ and can be expressed as $\Phi = \Phi(\chi) = \partial\Delta G/\partial\chi$, where ΔG is the excess intermolecular interaction energy per unit area. It is related to the dimensional conjoining pressure, ϕ ($\phi = \partial\Delta G/\partial\eta$, where $\eta = h - af$ is the dimensional local thickness), by $\Phi = (2\pi h_0^3/|A_e|)(\partial\Delta G/\partial\eta)$. Here A_e is the effective Hamaker constant for the van der Waals interaction. Therefore, on a physically heterogeneous surface, a spinodally stable film may become unstable whenever the condition $\partial\Delta G/\partial\chi < 0$ is satisfied at any local thickness. We consider here the simplest potential that can describe a thin liquid film subjected to the long-range intermolecular forces with the cut off for the attractive van der Waals forces provided by the very short-range repulsive forces with coefficient B.[14]

$$\Delta G = -(A_e/12\pi\eta^2) + (B/\eta^8) \quad (2)$$

Eqn (1) is numerically solved using a central difference scheme in space (X and Y) combined with Everett interpolation method and periodic boundary conditions at the edges. Gear's algorithm for stiff equations is employed for the time marching. In all the simulations, the initial configuration ($T = 0$) of the film is kept conformal with the substrate topography. The grid spacing is

always kept uniform ($\Delta X = \Delta Y$) in this study, and convergence of results is verified by increasing the grid density.

Conclusions

Dewetting of a thin polymer film on a patterned substrate can be used as a rapid, powerful, reproducible and simple technique for aligning and ordering of mesoscale structures over large areas ($\sim$cm^2). We show one to two orders of reduction in the magnitude of feature size compared to the spinodal length-scale by a severe lateral confinement imposed by the substrate patterns. In contrast to the earlier studies on the dewetting of spin-coated films on topographically patterned substrates, we have used a transferred film of uniform thickness. It is thus shown that in contrast to the spin coated films, the length-scale and the positioning of the final dewetted structures can be entirely controlled by the topography of the substrate rather than by the spinodal length-scale. Further, positioning of the dewetted structures can be tuned by varying the initial configuration of the transferred films. On a 2-D patterned substrate consisting of an array of square posts, the dewetted droplets self-organize at the channel intersections for a conformally adhering film, but form on pillar tops for a focally adhering film of the same thickness.

For a conformally adhering film, two distinct dewetting pathways are seen. For ultra-thin and moderately thin films ($\lesssim$40 nm), the film rupture is correlated to the underlying pattern. The experiments and simulations in this case show increased filling of the interstitial spaces with an increase in the film thickness. In addition, simulations suggest two different dewetting pathways in the cases of the overflow and under-filling of the interstitial spaces. A perfectly filled and ordered structure occurs only for a narrow window of film thicknesses. For the lower film thickness out of this window, the dewetting film fails to produce a droplet at each interstitial site resulting in imperfect order. Dewetting of thicker films shows spilling of droplets into the channels forming some inter-connected droplets.

For still thicker films (>40 nm), dewetting is nucleated with the formation of random holes completely non-correlated to substrate patterns. The contact line of the growing holes undergoes a stick–slip motion, which leaves behind an isolated polymer droplet at each interstitial corner, thus forming a multi-scale pattern. The pattern now consists of a perfectly filled and ordered array of sub-micron polymer droplets at channel intersections and large, randomly distributed droplets ($\sim$10 microns in diameter) because of hole coalescence. Thus, the perfect filling and ordering which is lost outside a window of the film thickness (17–25 nm on a type 1 substrate) is again regained for much thicker films (>40 nm) because of another pathway of dewetting. It is also shown that dewetting of a film on more intricate substrates can lead to the formation of more complex ordering in the final structure, which is evident from the "star" shaped array obtained on a substrate comprising an alternate array of rhombic zones.

Thus, pattern-directed dewetting of a thin polymer film leads to a myriad of structures, depending on the film preparation conditions, initial thickness and morphology of the film, geometry and periodicity of the substrate. Furthermore, ordered structures both perfectly correlated and uncorrelated to the substrate topography can be tailored. Finally, removal of the limitations imposed by the long spinodal length-scale allows the limit of miniaturization dictated by the underlying substrate to be attained. Formation of such patterned structures with micron or sub-micron sized features are likely to be relevant in many technologically important areas, for example creation of super-hydrophobic surfaces, where the dewetted patterns are likely to provide surface roughness causing superhydrophobicity.[62]

Acknowledgements

AS acknowledges the support of the DST through its grants to the Unit on Nanosciences at IIT Kanpur, J. C. Bose Fellowship and an IRHPA grant.

References

1 G. Reiter, *Phys. Rev. Lett.*, 1992, **68**, 75.
2 G. Reiter, *Langmuir*, 1993, **9**, 1344.
3 F. Brochard, P.-G. de Gennes, H. Hervet and C. Redon, *Can. J. Phys.*, 1990, **68**, 1084.
4 F. Brochard-Wyart, J.-M. di Meglio, D. Qu'er'e and P.-G. De Gennes, *Langmuir*, 1991, **7**, 335.
5 R. Yerushalmi-Rozen and J. Klein, *Langmuir*, 1995, **11**, 2806.
6 R. Yerushalmi-Rozen, T. Kerle and J. Klein, *Science*, 1999, **285**, 1254.
7 U. Steiner, J. Klein, E. Eiser, A. Budkowski and L. J. Fetters, *Science*, 1992, **258**, 1126.
8 U. Steiner, J. Klein and L. J. Fetters, *Phys. Rev. Lett.*, 1994, **72**, 1498.
9 M. D. Morariu, E. Schaffer and U. Steiner, *Phys. Rev. Lett.*, 2004, **92**, 156102.
10 R. Seeman, S. Herminghaus and K. Jacobs, *Phys. Rev. Lett.*, 2001, **86**, 5534.
11 J. Becker, G. Grun, R. Seemann, H. Mantz, K. Jacobs, K. R. Mecke and R. Blossey, *Nat. Mater.*, 2003, **2**, 59.
12 A. Sharma and G. Reiter, *J. Colloid Interface Sci.*, 1996, **178**, 383.
13 A. Sharma and R. Khanna, *Phys. Rev. Lett.*, 1998, **81**, 3463.
14 A. Ghatak, R. Khanna and A. Sharma, *J. Colloid Interface Sci.*, 1999, **212**, 483.
15 G. Reiter, R. Khanna and A. Sharma, *Phys. Rev. Lett.*, 2000, **85**, 1432.
16 A. Sharma, *Eur. Phys. J. E*, 2003, **12**, 397.
17 R. Verma and A. Sharma, *Ind. Eng. Chem. Res.*, 2007, **46**, 3108.
18 G. Reiter, M. Hamieh, P. Damman, S. Sclavons, S. Gabriele, T. Vilmin and E. Raphael, *Nat. Mater.*, 2005, **4**, 754.
19 L. Brusch, H. Kühne, U. Thiele and M. Bär, *Phys. Rev. E*, 2002, **66**, 011602.
20 U. Thiele, L. Brusch, M. Bestehorn and M. Bär, *Eur. Phys. J. E*, 2003, **11**, 255.
21 J. C. T. Kao, A. A. Golovin and S. H. Davis, *J. Colloid Interface Sci.*, 2006, **303**, 532.
22 M. Cavallini, M. Facchini, M. Massi and F. Biscarini, *Synth. Met.*, 2004, **146**, 283.
23 S. Luan, Z. Cheng, R. Xing, Z. Wang, X. Yu and Y. Han, *J. Appl. Phys.*, 2005, **97**, 086102.
24 J. Z. Wang, Z. H. Zheng, H. W. Li, W. T. S. Huck and H. Sirringhaus, *Nat. Mater.*, 2004, **3**, 171.
25 R. Konnur, K. Kargupta and A. Sharma, *Phys. Rev. Lett.*, 2000, **84**, 931.
26 K. Kargupta, R. Konnur and A. Sharma, *Langmuir*, 2000, **16**, 10243.
27 M. Zope, K. Kargupta and A. Sharma, *J. Chem. Phys.*, 2001, **114**, 7211.
28 K. Kargupta and A. Sharma, *Phys. Rev. Lett.*, 2001, **86**, 4536.
29 K. Kargupta and A. Sharma, *Langmuir*, 2001, **17**, 1294.
30 K. Kargupta and A. Sharma, *J. Colloid Interface Sci.*, 2002, **245**, 99.
31 K. Kargupta and A. Sharma, *Langmuir*, 2002, **18**, 1893.
32 K. Kargupta and A. Sharma, *J. Chem. Phys.*, 2002, **116**, 3042.
33 K. Kargupta and A. Sharma, *Langmuir*, 2002, **19**, 5153.
34 A. Sharma, R. Konnur and K. Kargupta, *Physica A*, 2003, **318**, 262.
35 D. Simmons and A. Chauhan, *J. Colloid Interface Sci.*, 2006, **295**, 472.
36 A. M. Higgins and R. A. L. Jones, *Nature*, 2000, **404**, 476.
37 X. Zhang, F. Xie and O. K. C. Tsui, *Polymer*, 2005, **46**, 8416.
38 H. G. Braun and E. Mayer, *Thin Solid Films*, 1999, **345**, 222.

39 H. G. Braun and E. Mayer, *Macromol. Mater. Eng.*, 2000, **276/277**, 44.
40 A. Sehgal, V. Ferreiro, J. F. Douglas, E. J. Amis and A. Karim, *Langmuir*, 2002, **18**, 7041.
41 D. Julthongpiput, W. Zhang, J. F. Douglas, A. Karim and M. J. Fasolka, *Soft Matter*, 2007, **3**, 613.
42 Z. Zhang, Z. Wang, R. Xing and Y. Han, *Polymer*, 2003, **44**, 3737.
43 Z. Zhang, Z. Wang, R. Xing and Y. Han, *Surf. Sci.*, 2003, **539**, 129.
44 X. Wang, M. Ostblom, T. Johansson and O. Inganas, *Thin Solid Films*, 2004, **449**, 125.
45 X. Wang, K. Tvingstedt and O. Inganas, *Nanotechnology*, 2005, **16**, 437.
46 N. Rhese, C. Wang, M. Hund, M. Geoghegan, R. Magerle and G. Krausch, *Eur. Phys. J. E*, 2001, **4**, 69.
47 M. Geoghegan, C. Wang, N. Rhese, R. Magerle and G. Krausch, *J. Phys.: Condens. Matter*, 2005, **17**, S389.
48 C. Luo, R. Xing, Z. Zhang, J. Fu and Y. Han, *J. Colloid Interface Sci.*, 2004, **269**, 158.
49 R. Mukherjee, M. Gonuguntla and A. Sharma, *J. Nanosci. Nanotechnol.*, 2007, **7**, 2069.
50 R. Xing, C. Luo, Z. Wang and Y. Han, *Polymer*, 2007, **48**, 3574.
51 K. Y. Suh and H. H. Lee, *J. Chem. Phys.*, 2001, **115**, 8204.
52 K. Y. Suh, J. Park and H. H. Lee, *J. Chem. Phys.*, 2002, **116**, 7714.
53 K. Y. Suh and H. H. Lee, *Adv. Mater.*, 2002, **14**, 346.
54 S. Harkema, E. Schaffer, M. D. Morariu and U. Steiner, *Langmuir*, 2003, **19**, 9714.
55 C. Luo, R. Xing and Y. Han, *Surf. Sci.*, 2004, **552**, 139.
56 Y. S. Kim and H. H. Lee, *Adv. Mater.*, 2003, **15**, 332.
57 D. H. Kim, M. J. Kim, J.-Y. Park and H. H. Lee, *Adv. Funct. Mater.*, 2005, **15**, 1445.
58 E. Ruckenstein and R. K. Jain, *J. Chem. Soc., Faraday Trans. 2*, 1974, **70**, 132.
59 R. Mukherjee, M. Gonuguntla and A. Sharma, *J. Nanosci. Nanotechnol.*, 2008, DOI: 10.1166/jnn.2008.121.
60 M. Gonuguntla, A. Sharma, R. Mukherjee and S. A. Subramanian, *Langmuir*, 2006, **22**, 7066.
61 A. Sharma, M. Gonuguntla, R. Mukherjee, S. A. Subramanian and R. C. Pangule, *J. Nanosci. Naotechnol.*, 2007, **7**, 1744.
62 P. van der Wal and U. Steiner, *Soft Matter*, 2007, **3**, 426.